www.cadanda.com
Computer-Aided Design AND APPLICATIONS

Towards the Integration of Topology Optimization into the CAD Process

Jean-Christophe Cuillière[1], Vincent Francois[1] and Jean-Marc Drouet[2]

[1]Université du Québec à Trois-Rivières, Canada, cuillier@uqtr.ca, francois@uqtr.ca
[2]Université de Sherbrooke, Canada, Jean-Marc.Drouet@usherbrooke.ca

ABSTRACT

This paper presents a contribution to the automation and integration of topology optimization methods (TOM) with CAD, in the context of the design of statically loaded mechanical structures and parts. Starting from an initial CAD model with relevant engineering data, the goal is automatically generating an optimized CAD model with respect to engineering objectives and constrains. Though many optimization methods are now available, their complete and efficient integration into the design process faces several problems. After introducing the basic steps involved in the whole process and identifying the challenges inherent to this integration, this paper presents our contribution in addressing these challenges. The paper is focused on the specification of *design and non-design sub-domains*, on automatic mesh generation problems induced and on the adaptation of TO concepts in the context of 3D unstructured meshes. TO itself is adapted from a SIMP scheme, which is an arbitrary choice as any other optimization method could also have been used. Sets of results are presented to illustrate the potential and difficulties inherent to integrating TOM into the product design process with CAD.

Keywords: topology optimization, B-Rep, CAD/FEA integration, SIMP method, mesh generation, multiple domains.

1. INTRODUCTION: THE TOPOLOGY OPTIMIZATION PROCESS

Finite element analysis (FEA) has proven its potential when trying to optimize stiffness of parts assemblies and structures. Optimizing stiffness is usually performed with the objective of minimizing weight, which means modifying an initial geometry, while insuring to sustain prescribed loads, applied on this evolving geometry. Several methods have been introduced to automate this optimizations process. These methods are mainly based on applying FEA to shapes that are evolving automatically. Input data required at the beginning of the optimization process typically stands as an initial 3D geometry added with the specification of material which should not be affected by the optimization process (referred to as *non-design material*) and loads, boundary conditions (BC) and material data. From this starting point, the objective is automating the transformation of the initial shape and topology into an optimized shape and topology with respect to size, weight, strength and eventually stiffness. Towards this objective, topology optimization methods (TOM) [1,2,4,6,12,15,16] has been a field of promising and active research for the last fifteen years. The great potential of TOM is that the evolution of shape and topology is not necessarily constrained by the topology of the initial domain. Thus, the resulting topology obtained at the end of the process is not known a priori, which somehow tends to automate the production of new design ideas. Bringing this technology to maturity is likely to open a new era for product development with computer aided design (CAD). In fact, the evolution of geometric modeling, automatic mesh generation and TOM now allows foreseeing the actual integration of TO into the product design process and by the way, sets up the conditions for its wider use. Fig. 1 presents a general framework for the integration of TO technology into the CAD world and the overall process can be synthesized by considering the following basic steps.

It starts with providing the automatic optimization process with the input data required (initial geometry, loads, BC and material properties). In the context of TO, the initial geometry must me defined in a specific way because the optimization process must globally affect its shape and topology while respecting the functional integrity of some subsets of this initial geometry. For example, material around fastening

Computer-Aided Design & Applications, 11(2), 2013, 120–140, http://dx.doi.org/10.1080/16864360.2014.846067

Taylor & Francis

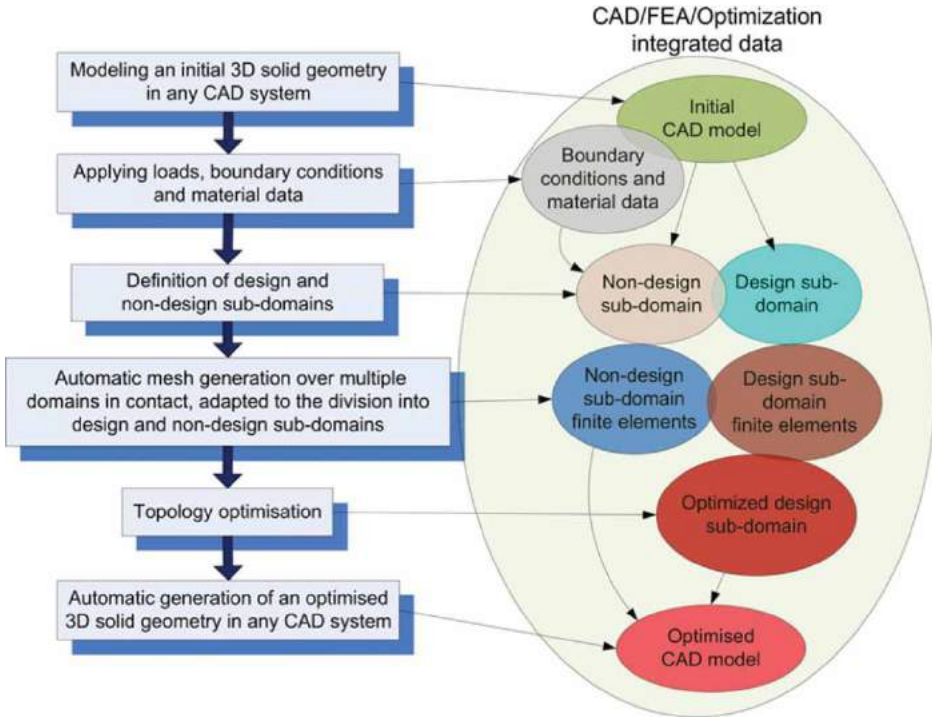

Fig. 1: A scheme of the topology optimization process.

holes or, more generally, material around geometric features on which loads or BC are applied should not be modified by the TO process. All these subsets of the initial geometry, that must be kept intact for whatever reason, are referred to as the *non-design sub-domain*. The remainder of the initial geometry is composed with material which is likely, on the contrary, to be remodeled by TO and it is referred to as the *design sub-domain*. Of course, for a given case, the Boolean union of *design* and *non-design* sub-domains results in the whole initial domain and the Boolean intersection between *design* and *non-design* sub-domains is a null volume. Then, as explained in the following sections, this specific partition of the initial geometry implies using specific mesh generation procedures so that the mesh of the initial geometry is also partitioned into design and non-design finite elements. Consequently, during the TO process itself, elements tagged as non-design elements will not be affected while the process will only operate on elements tagged as design elements. Then, the result provided by the TO process itself is a 3D shape composed with the union of the non-design sub-domain and an evolution or optimization of the design sub-domain. It must be underlined here that some TO processes only remove design material from the initial design domain while others both remove and add design material.

This paper brings about some new ideas and tools intended to contribute to the objective of fully automating the optimization of statically loaded 3D mechanical parts and structures. We will basically present how geometric modeling and mesh generation concepts can be successfully adapted and integrated with TOM towards this objective. In this work, this integration is basically performed through specific adaptations of advancing front automatic mesh generation and transformation algorithms and adaptations of boundary representation (B-Rep) concepts. Also, TO in itself is based on the solid isotropic material with penalization (SIMP) method [1,2,16], which is a very standard optimization method. It is very important to underline that this choice *is arbitrary and that many other optimization methods could have been considered instead*. The authors are well aware that commercial codes and systems are developed towards similar objectives (ex.: TOSCA by FE-Design GmbH, OptiStruct by Altair Engineering Inc.). However, none of the research work behind these products is available in the literature. Our approaches and research results are therefore presented in this paper for the benefit of the larger scientific community.

The paper is organized as follows. Section 2 lists the challenges of automating the TO process and integrating it into the design process with CAD. Section 3 presents our contribution to this integration through several sub-sections which are related to the successive steps of the overall process and section 4 illustrates, with several practical examples, the potential and challenges encountered in integrating this technology with CAD. The paper ends with a conclusion and perspectives.

2. AUTOMATION OF THE TOPOLOGY OPTIMIZATION PROCESS

Even if several papers [7,11,19] can be found in the literature, aimed at integrating TOM into the CAD process, the solutions presented are either limited to 2D shapes or fragmentary and lots of problems remain to be solved. Ideally, the process should automatically derive a 3D optimized CAD model from the input of an initial CAD model with relevant data (typically the non-design sub-domain, BC and relevant engineering data). This objective is very ambitious for different reasons and the full automation of the process presented in the previous section faces the following challenges:

- The easy and efficient definition of the non-design sub-domain: the specification of non-design material should be made by using a combination of automatic processing with interactive selection. In fact, the material located around geometric features of the initial CAD model on which some of the BC are applied can be automatically derived into subsets of the non-design sub-domain. However, the designer should also be provided with an efficient and interactive interface, allowing an easy selection of non-design geometry, directly on the initial CAD model. It will be shown in section 4.4 that the specification of non-design material with respect to BC applied is a key and sensitive issue in using TOM effectively because it has a direct and very significant impact on optimization results obtained at the end.
- The representation of the design and non design sub-domains: once specified the non-design sub-domain, design and non-design sub-domains must be saved and the representation used should be consistent with both requirements inherent in the partition of geometry applied (into design and non-design sub-domains) and requirements inherent in the specific mesh generation procedures used afterwards.
- The automatic generation of the initial geometry's mesh and its automatic partition into design and non-design finite elements. The partition of geometry (into design and non-design sub-domains), along with constraints on this partition, imply using specific adaptations of automatic mesh generation procedures. Also, even if many algorithms and approaches have been introduced to limit this impact [2,18], the mesh of the initial design sub-domain has a impact on optimization results, especially with respect to the degree of refinement of the final shape and topology. Consequently the problem is not simply generating a mesh (with the constraints aforementioned) but it is also generating a "good" mesh for obtaining "good" optimization results at the end.
- Integrating the TOM used (in our case the SIMP method) into the process. Since many optimization methods are introduced in 2D on structured meshes, the first challenge faced is adapting theses methods to 3D on unstructured meshes, which is a requirement towards automation of the whole process for 3D solid models. Another important issue is calibrating the optimization method used in order to obtain, at the end of the whole process, good optimization results with respect to practical engineering objectives. TOM involve many parameters and the optimized shape and topology obtained are strongly influenced by some of these parameters. Automation of the process requires a thorough study of these parameters' influence on the final result of the optimization process so that these parameters can then be automatically calibrated with regard to practical engineering concerns (the type of geometry and BC involved, the optimization's objective, manufacturing perspectives, etc.).
- Capturing a 3D shape and by the way practical design intent from results provided by TOM. Some TOM [6,15] try to incorporate explicit or implicit CAD geometry directly into the optimization problem but it at this point it is limited to 2D geometry. In fact, the result provided by 3D TOM does not directly and explicitly take the form of an optimized 3D shape. For example, the SIMP method (which is used in this paper) results in a 3D relative density distribution, which requires to be processed in order to obtain an actual 3D shape. Moreover, the challenge is wider than simply deriving an optimized 3D volume. Indeed, the main objective is capturing "load paths" (identified by the optimization process) that are likely to be derived into an optimized CAD model at the very end of the process. The way these "load paths" are modeled is fundamental because it has a direct impact on the way the final CAD model can be automatically built.
- Last but not least, the optimized 3D shape has to be derived automatically into an optimized 3D CAD model. This represents a very ambitious challenge because, to be consistent with the product development process, the optimized CAD model needs to be built with respect to its manufacturability. This means that optimization results must be transformed into smoothed and functional boundaries and that the final shape must be likely to be manufactured at a reasonable cost. Obviously, a significant compromise has to be made between the degree of optimization and the cost induced. Indeed, the optimal topology is likely to be very complex which is in contradiction with the objective of reducing manufacturing costs.

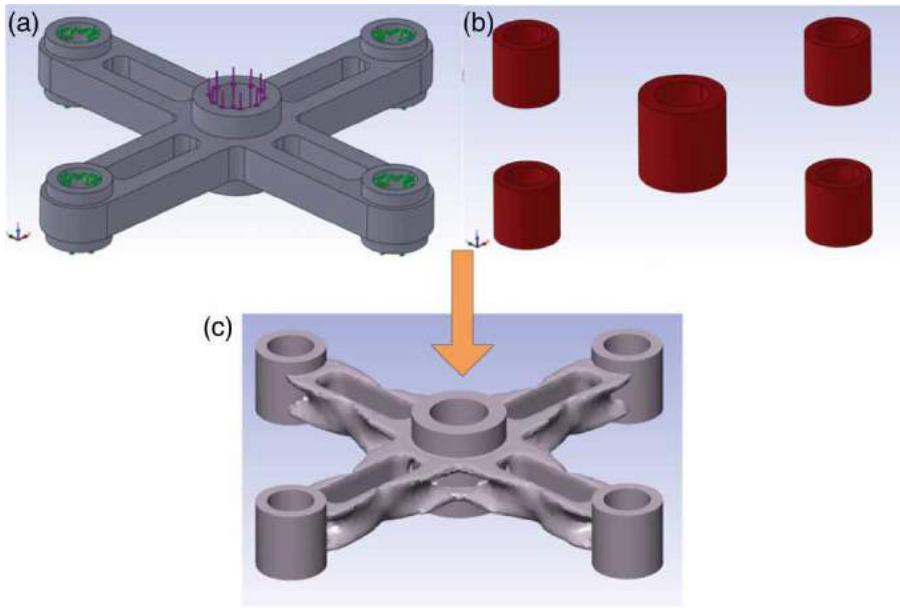

Fig. 2: A first topology optimization example: (a) the initial design with loads and BC, (b) the non-design sub-domain, (c) the result obtained with our topology optimization platform.

The work presented in this paper contributes to provide solutions to some of these challenges.

3. OUR CONTRIBUTION TO THE PROCESS

In sections 1 and 2 we have presented the basic steps of the optimization process and the challenges related to its automation. The next sections will describe with details our main contributions to this process which are:

- Defining and modeling design and non-design domains easily and efficiently.
- Setting up specific automatic 3D mesh generation and transformation tools. These tools are used upstream to TO (for the conformal meshing of design and non-design sub-domains) and downstream to TO (for the transformation of raw optimization results into a smooth and continuous optimized shape)
- Adapting the SIMP method to the context of 3D unstructured tetrahedral meshes.
- Studying the interaction between the specification of non-design sub-domains and BC and studying its impact on SIMP results.
- Studying the impact of SIMP parameters on 3D shapes and topology derived.

3.1. Modeling the Initial Geometry and Applying Loads, BC and Material Properties

This step is *a priori* straightforward as it consists of building an initial geometry in a CAD system and applying BC and material properties to this initial geometry. Practically, as this initial geometry has a major impact on the final result, building a "good" initial geometry is not so easy. Moreover, TOM are likely to be used in the two following contexts:

- Fig. 2 illustrates an example for which TO is used to refine an initial design that already features a certain level of detail. The central hole is loaded vertically (in purple) and the four mounting holes are attached (null displacements are imposed in green). The initial design and final optimization result are respectively shown in Fig. 2a and Fig. 2c. Fig. 2b illustrates the material of the initial design that must not be affected by the optimization process (referred to in this work as the *non-design sub-domain*).
- Fig.3 illustrates a case where TO is applied on a very coarse initial shape, which demonstrates its potential in creating new design ideas "from scratch". Loads and BC are the same as in the previous example and the initial design and final optimization result are respectively shown in Fig. 3a and Fig. 3c. Fig. 3b illustrates the *non-design sub-domain*.

For both of these two examples, the final amount of material is the same but the optimized results obtained at the end are obviously quite different. These two examples illustrate that TO can be used in very different contexts and that being in one or another context usually has a major impact on final optimization results obtained.

3.2. Specifying Non-design Sub-domains

As mentioned previously the optimization process improves the shape and topology of an initial domain

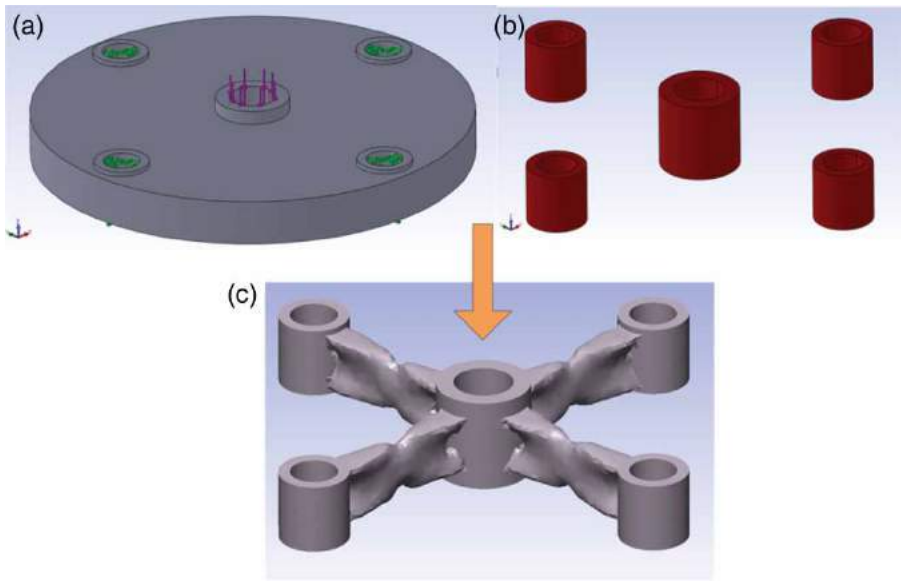

Fig. 3: A second topology optimization example: (a) the initial design with loads and BC applied, (b) the non-design sub-domain, (c) the result obtained using our integrated topology optimization platform.

while maintaining intact some subsets of this initial domain throughout the whole process. Sets of 3D sub-volumes of the initial geometry, referred to as the *non-design sub-domain*, have to be specified and processed differently. This involves a significant increase of complexity when trying to integrate the optimization process itself with CAD and as illustrated in section 4.4, it has a major impact on optimization results obtained at the end. At this stage of our research, the *non-design sub-domain* for a given part is defined using a specific boundary representation (B-Rep) model, which is added to the B-Rep associated with the entire domain. B-Rep is a very classical data structure aiming at a concise representation of solid geometry [14] and it is widely used in the contexts of 3D modeling and visualization. Fig. 4 illustrates our way of specifying non-design sub-domains. A first B-Rep structure (Fig. 4a) describes the entire geometry and a second B-Rep structure (Fig. 4b) describes the non-design sub-domain. The *design sub-domain* is shown in Fig. 4c but it is not defined explicitly. In fact, it does not have to be defined explicitly. In our work indeed, the design sub-domain is implicitly defined through a specific mesh generation process (introduced in the next section). As shown in Fig. 4b for the non design sub-domain, it appears in general that both design and non-design sub-domains B-Rep structures are likely to feature several separate bodies even if the initial B-Rep structure of the whole part is usually composed of a unique body (except in some specific cases such as multi-material parts).

3.3. Meshing Multiple Sub-domains in Contact

As mentioned in the previous paragraph, design and non-design sub-domains are defined using two separate CAD models, one associated with the entire model and the other one with non-design geometry. This specific and mandatory definition of geometry implies using of specific mesh generation procedures so that finite elements generated (linear tetrahedrons in this work) can be tagged as *design elements* and *non design elements*. This identification of elements as design and non-design elements allows the optimization process itself to apply on design elements only and to keep non-design elements unchanged. Also, the mesh of design and non-design geometry must be performed so that continuity and conformity of the mesh, at the interface between design and non-design geometry, should be guaranteed. These two requirements (tagging tetrahedron elements and insuring mesh conformity at interfaces) make that standard automatic mesh generation procedures [9] have to be adapted, which is referred to, in the literature, as mesh generation over multiple domains in contact or as mesh generation for domains with multiple materials [8,13,20]. In this work, automatically filling multiple domains in contact with tetrahedrons is performed using specific mesh generation procedures as developed by our research team. Basically, these procedures consist of extending standard advancing front mesh generation (AFM) principles to the context of meshing multiple domains in contact. The overall mesh generation process (see reference [8] for the details) is divided into 14 basic steps, which are intended to make sure that the mesh of each sub-domain is performed with respect to constraints imposed by the mesh of the other sub-domains. The principle that underlies this process is transferring mesh elements (nodes, lines, triangles and tetrahedrons) from one B-Rep model to the other one and so on. At the end, this back and forth process insures

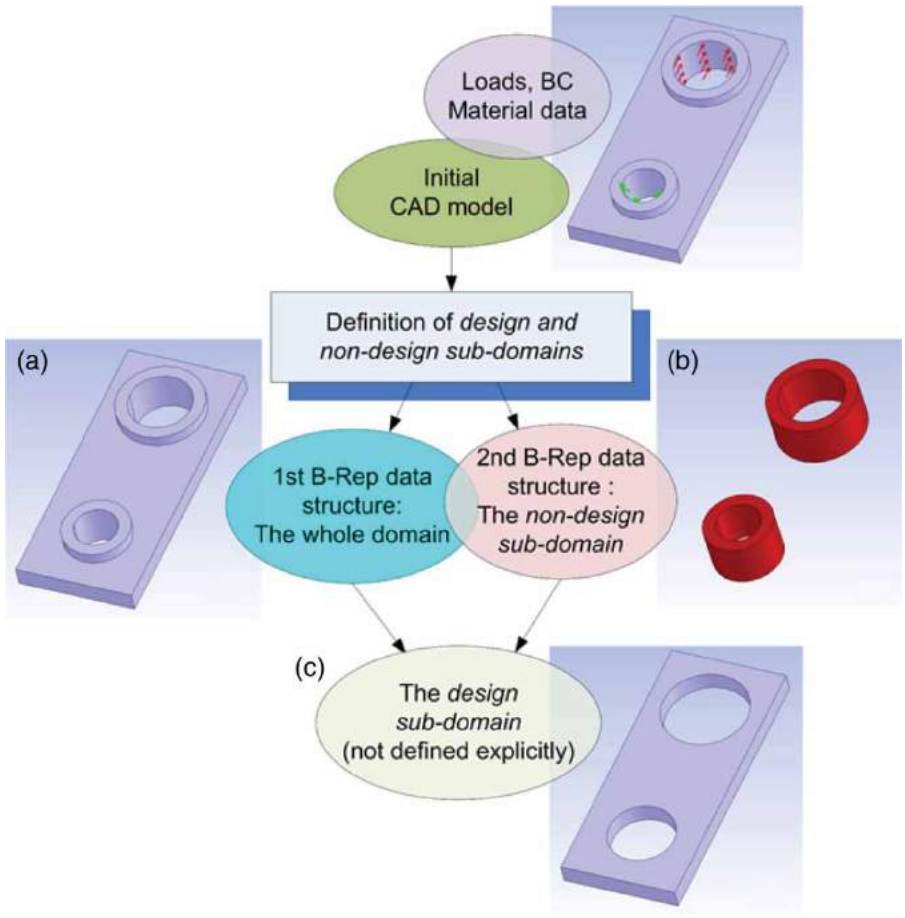

Fig. 4: Definition of design and non-design sub-domains: (a) the entire domain, (b) the non-design sub-domain, (c) the design sub-domain.

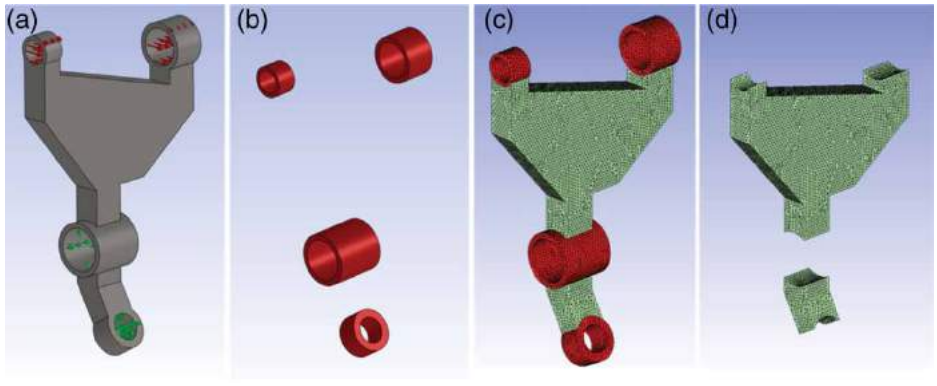

Fig. 5: (a) A bike suspension rocker with loads and BC, (b) the non-design sub-domain, (c) the resulting mesh, (d) Implicit definition of the design domain.

the conformity and continuity of the resulting mesh. Fig. 5c illustrates the mesh obtained on a bike suspension rocker. Fig. 5a presents the initial model along with loads and BC and Fig. 5b presents the non-design model, which is composed with zones of the rocker that are in contact with other parts in the assembly of the suspension. As mentioned before, geometry of the design sub-domain is not defined explicitly and it does not have to. Indeed, once this specific mesh generation algorithm applied, the design sub-domain is implicitly defined as the volume filled with design tetrahedrons, as shown in Fig. 5d. This heterogeneous and unstructured mesh along with loads, BC, material data and optimization parameters, is transferred, as input, to the TO process itself.

3.4. An Adaptation of the SIMP Method to 3D Unstructured Meshes

3.4.1. The SIMP method

In this work, as presented in the next section, TO is adapted from a classical solid isotropic material with penalization (SIMP) scheme. This is an arbitrary choice as many other optimization methods could also have been used successfully (ESO, BESO, SINH, level-set based, etc.). The foundation principle of the SIMP method is computing an iterative evolution of the spatial distribution of material porosity across the design sub-domain. The global amount of porosity (or void) is prescribed as an input of the SIMP process and it is kept constant throughout the iterations. Thus, explained with very simple words, the SIMP method optimizes the distribution of a prescribed quantity of porosity (or void) that is removed from the initial design towards the objective of maximizing the design's stiffness. The distribution of porosity is mathematically represented by a relative density field $\rho(x, y, z)$. Relative density varies from 0 (no material) to 1 ("full" or actual material) and it is derived into the distribution of a virtual elastic modulus $\tilde{E}(x, y, z)$, according to the penalisation law $\tilde{E}(x, y, z) = E.\rho(x, y, z)^p$ (E is the actual material's elastic modulus and p an integer penalization coefficient that is usually chosen between p = 1 and p = 3). As we will use it in the following equations, a classical convention in the mathematical description of the SIMP method is that all objects that are affected by the relative density field $\rho(x, y, z)$ are noted using a $\sim$. Also, as non-design material should not be affected by the optimization process, $\rho = 1$ is imposed inside the non-design sub-domain throughout the iterations. The objective of the SIMP process is iteratively searching for a distribution of $\rho(x, y, z)$ that maximizes stiffness or in other words, that minimizes the domain's global compliance $\tilde{C}$. Using a finite element discretization and introducing the equilibrium equation $[\tilde{K}].\{\tilde{U}\} = \{F\}$, the global compliance is defined (with for the virtual material distribution) as the scalar:

$$\tilde{C} = \{\tilde{U}\}^t.\{F\} = \{\tilde{U}\}^t.[\tilde{K}].\{\tilde{U}\}$$

$\{\tilde{U}\}$ is the global displacement vector (affected by $\rho(x, y, z)$) and $[\tilde{K}]$ the global stiffness matrix (also affected by $\rho(x, y, z)$). $\{F\}$ is the global vector associated with forces applied (not affected by $\rho(x, y, z)$).

If we consider that the mesh is composed with N elements and that the local stiffness matrix of element e for $\rho = 1$ (full or actual material) is $[K^e]$, then we can define for this element a modified stiffness matrix $[\tilde{K}_e]$, due to the impact of the relative density ρ_e inside the element:

$$[\tilde{K}_e] = (\rho_e)^p.[K_e]$$

By the way, the global stiffness matrix $[\tilde{K}]$ is $[\tilde{K}] = \sum_{e=1}^{N}[\tilde{K}_e] = \sum_{e=1}^{N}(\rho_e)^p.[K_e]$

Thus, the global compliance $\tilde{C}$, once applied the relative density field, can be written as:

$$\tilde{C} = \{\tilde{U}\}^t.[\tilde{K}].\{\tilde{U}\} = \{\tilde{U}\}^t.\left(\sum_{e=1}^{N}(\rho_e)^p.[K_e]\right).\{\tilde{U}\}$$

$$= \sum_{e=1}^{N}(\rho_e)^p.\{\tilde{U}\}^t.[K_e].\{\tilde{U}\}$$

Practically, this global compliance is computed using the total strain energy $\tilde{W}$ as $\tilde{C} = 2.\tilde{W}$.

As already mentioned, a constraint imposed on the global amount of porosity, while trying to minimize $\tilde{C}$. This constraint is practically applied on the total volume fraction f, defined as $f = \frac{\tilde{V}}{V_d}$

$\tilde{V}$ is the design material volume affected by "porosity" and V_d is the total design material volume, which means the actual volume (without "porosity") of design material before beginning the SIMP process.

Thus the optimization problem can be formulated as:

$$\text{minimize } \tilde{C} = \sum_{e=1}^{N}(\rho_e)^p.\{\tilde{U}\}^t.[K_e].\{\tilde{U}\}$$

$$\text{with } \frac{\tilde{V}}{V_d} = f$$

$$[\tilde{K}].\{\tilde{U}\} = \{F\}$$

$$0 \leq \rho \leq 1$$

3.4.2. Adaptation of the SIMP method for 3D unstructured meshes

As mentioned in the introduction, our work is focused on integrating TOM in the product development process with CAD. As introduced in the previous section, it is easy to understand that automating the generation of a conformal mesh over design and non-design sub-domains of reasonable complexity can only be achieved through 3D unstructured mesh generation. The SIMP method has been initially introduced in the context of regular structured meshes (with constant or nearly constant sized and shaped quadrangles in 2D and hexahedra in 3D) and using it with unstructured meshes requires several adaptations on the one hand. On the other hand, this adaptation allows using meshes with steep variations in element sizes. This is practically very interesting because being able to use unstructured meshes with non-constant element sizes allows a local control on TO results (for example locally refining or coarsening the level of geometric details desired). With this objective, we have adapted the SIMP scheme presented in [2] to 3D unstructured tetrahedral meshes. First, at each iteration in the SIMP process, the field ρ is modified using the Optimality Criteria (OC) algorithm. ρ_e is modified through the

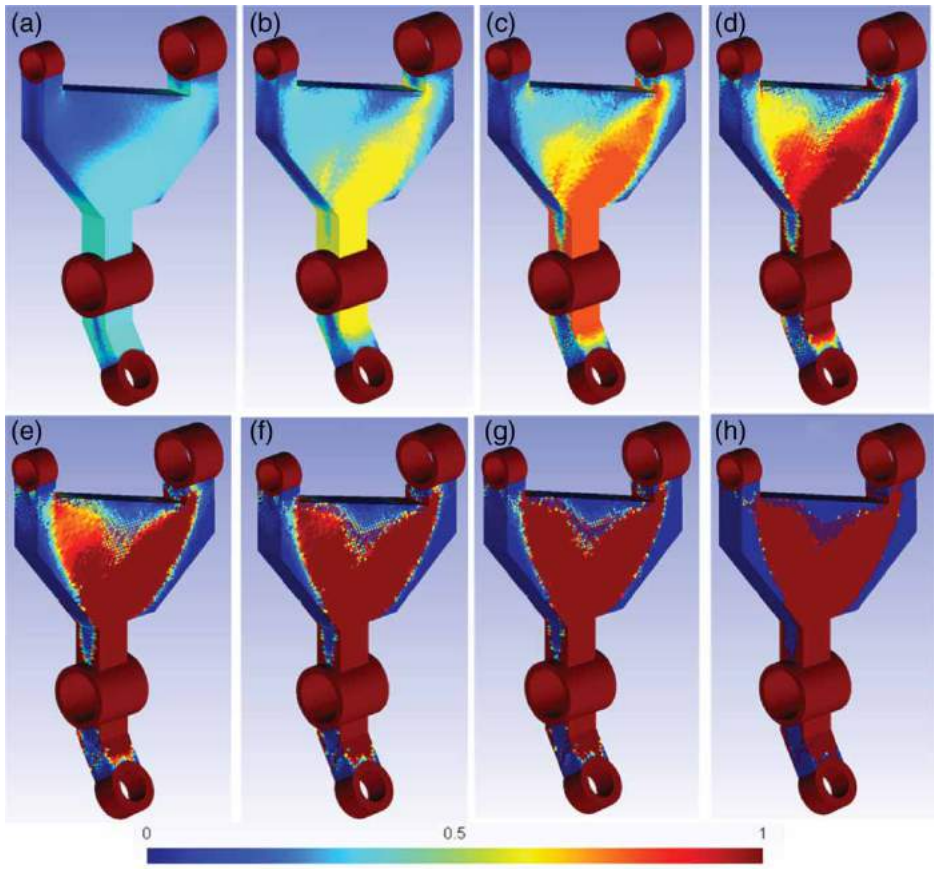

Fig. 6: Evolution $\rho(x,y,z)$ for the example in Fig. 5, after (a) 1 iteration (b) 2 iterations (c) 3 iterations (d) 4 iterations (e) 5 iterations (f) 6 iterations (g) 7 iterations (h) 12 iterations (with no filter applied).

following equation:

$$\rho_e^{new} = \begin{cases} \max(\rho_{void}, \rho_e - m) & \text{if } \rho_e\beta_e^\eta \le \max(\rho_{void}, \rho_e - m) \\ \rho_e\beta_e^\eta & \text{if} \max(\rho_{void}, \rho_e - m) < \rho_e\beta_e^\eta < \min(1, \rho_e + m) \\ \min(1, \rho_e + m) & \text{if} \min(1, \rho_e + m) \le \rho_e\beta_e^\eta \end{cases}$$

where ρ_e is the previous relative density inside element e and ρ_e^{new} is the updated (or new) relative density inside element e
m is a threshold on the variation of ρ_e and consequently $|\rho_e^{new} - \rho_e| \le m$ (practically, we used $m = 0.2$ for the examples presented in section 4
$\eta = \frac{1}{2}$ is a damping coefficient
ρ_{void} corresponds to a "numerical" void (for the results presented, the practical value of ρ_{void} is 10^{-3}).
β_e is calculated using the following equation:

$$\beta_e = \frac{-\frac{\partial \tilde{C}}{\partial \rho_e}}{\lambda \frac{\partial \tilde{V}}{\partial \rho_e}}$$

$\frac{\partial \tilde{C}}{\partial \rho_e}$ is the global compliance's sensitivity with respect to ρ_e, calculated from:

$$\frac{\partial \tilde{C}}{\partial \rho_e} = -\frac{p}{\rho_e}.\{\tilde{U}\}^t.[\tilde{K}_e].\{\tilde{U}\}$$

Practically, $\{\tilde{U}\}^t.[\tilde{K}_e].\{\tilde{U}\}$ is provided by FEA results, using the total strain energy inside element e, $\tilde{W}_e$ as $\{\tilde{U}\}^t.[\tilde{K}_e].\{\tilde{U}\} = 2.\tilde{W}_e$ and consequently:

$$\frac{\partial \tilde{C}}{\partial \rho_e} = -\frac{2.p.\tilde{W}_e}{\rho_e}$$

From $\tilde{V} = \sum_{e=1}^N \tilde{V}_e = \sum_{e=1}^N \rho_e.V_e$ we calculate $\frac{\partial \tilde{V}}{\partial \rho_e} = \frac{\partial \tilde{V}_e}{\partial \rho_e} = V_e$ which leads to $\beta_e = \frac{2.p.\tilde{W}_e}{\lambda.\rho_e.V_e}$

In this equation, λ is a Lagrange multiplier, calculated using a bisection algorithm which aims at adjusting the value of λ so that the volume fraction constraint is satisfied:

$$\tilde{V}(\rho) = \sum_{e=1}^N \rho_e^{new}.V_e = f.V_d$$

At each iteration, element densities ρ_e are updated and a FEA is performed to calculate the updated global compliance $\tilde{C}_i$ ($\tilde{C}_i$ is the global compliance at iteration *i*). The iterative process stops when a threshold on $\Delta_i = \frac{\tilde{C}_i - \tilde{C}_{i-1}}{\tilde{C}_{i-1}}$, the relative variation of $\tilde{C}_i$ between two consecutive iterations is reached.

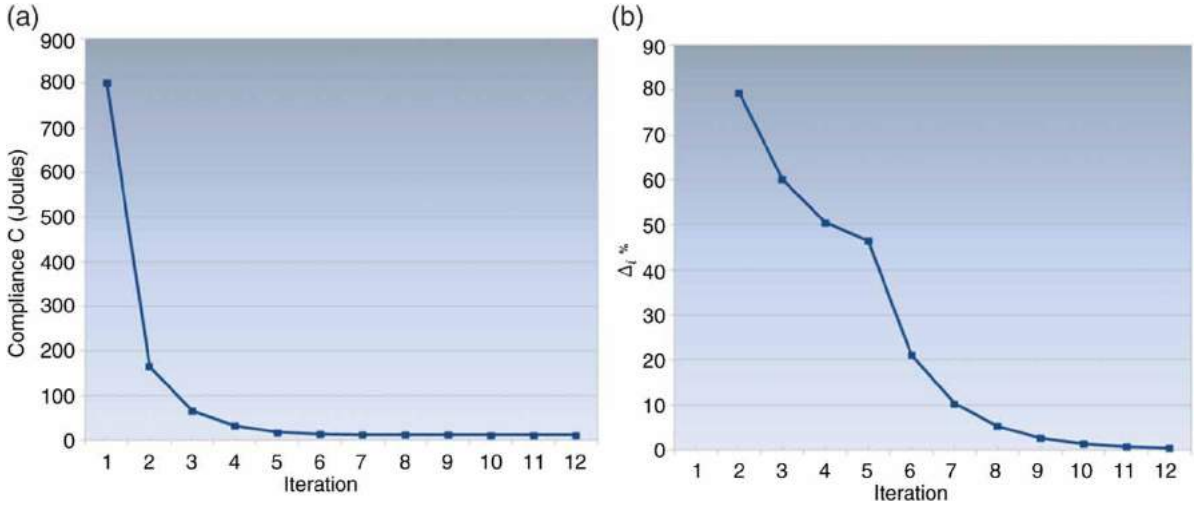

Fig. 7: For the example in Fig. 6 (a) Evolution of $\tilde{C}_i$ along SIMP iterations (b) Evolution of Δ_i along SIMP iterations.

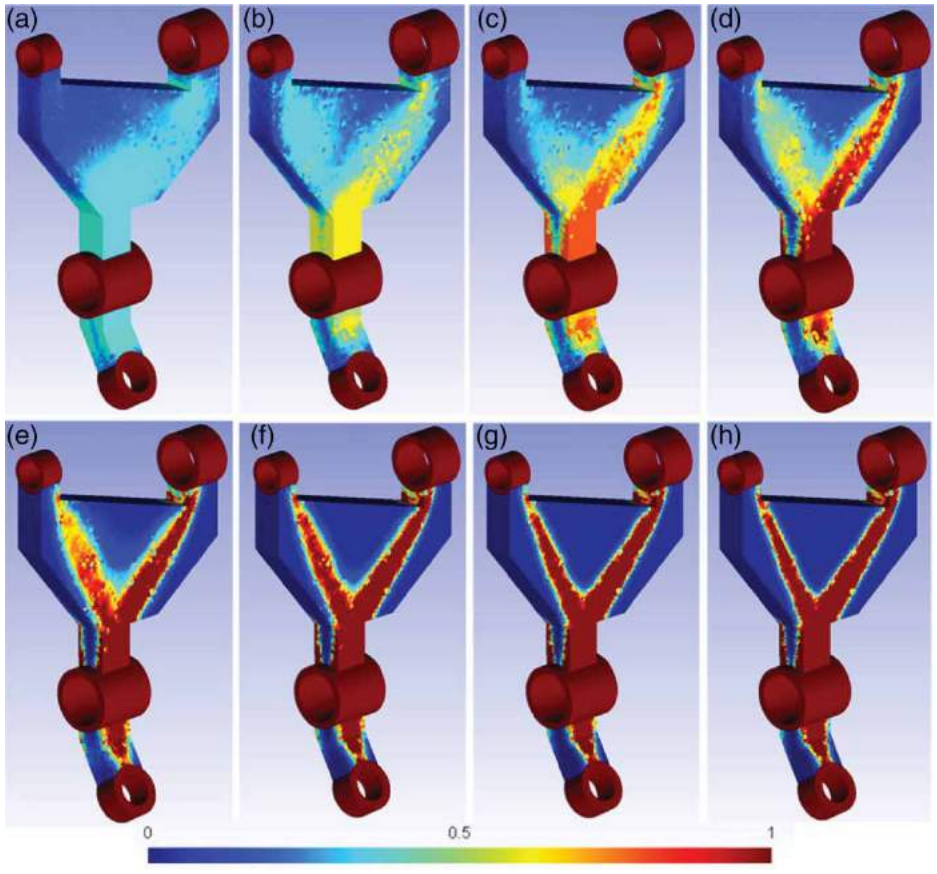

Fig. 8: Evolution $\rho(x, y, z)$ for the example in Fig. 5, after (a) 1 iteration (b) 2 iterations (c) 3 iterations (d) 4 iterations (e) 6 iterations (f) 8 iterations (g) 11 iterations (h) 16 iterations (with a filter on $\frac{\partial \tilde{C}}{\partial \rho_e}$ applied).

Fig. 6 illustrates, using the color scale shown at the bottom, 8 stages in the evolution of $\rho(x, y, z)$ for the example introduced in Fig. 5. Fig. 7a illustrates, for this example, the evolution of $\tilde{C}_i$ and Fig. 7b the evolution of Δ_i along SIMP iterations. In this case, convergence is achieved after 12 iterations when Δ_i is less than 0.5 %. It is obvious that the global compliance (Fig. 7a) and the distribution of $\rho(x, y, z)$ (Fig. 6) do not

	Without filtering	With a filter on $\frac{\partial \tilde{C}}{\partial \rho_e}$	With a filter on ρ_e
Number of iterations	12	16	21
Final compliance (Joules)	11	16.4	28.3

Tab. 1: The effect of filtering on the speed of convergence and on the final compliance

change much after 5 or 6 iterations, which means that the optimized shape and topology is reached after very few iterations.

3.4.3. *Adaptation of SIMP results filtering for 3D unstructured meshes*

The result shown in Fig. 6 illustrates a typical example of the checkerboard effect obtained in the final distribution of $\rho(x, y, z)$ when no filtering is applied. This effect tends to create micro-structures in the optimized material (due to the FEA discretization scheme used) and it has been intensively studied and illustrated in the context of 2D structured meshes. It is interesting to see the checkerboard effect in the context of 3D unstructured meshes. Several methods have been introduced in the literature to avoid it for structured meshes [2–4,17]. Among these methods, the following two main approaches can be mentioned:

- Filtering the compliance's sensitivity $\frac{\partial \tilde{C}}{\partial \rho_e}$
- Directly filtering the relative density distribution ρ_e

Both methods consist of locally calculating and using (around a given finite element e) a weighted average of the quantity to be filtered ($\frac{\partial \tilde{C}}{\partial \rho_e}$ or ρ_e) for the next iteration of the SIMP process. Filtering $\frac{\partial \tilde{C}}{\partial \rho_e}$ or ρ_e are usually considered as two distinct alternatives even if they can easily be combined. As for the SIMP method itself, these filtering methods require adaptations in the context of unstructured meshes. The major adaptation required concerns the way the aforementioned weighted average is calculated. In both cases the weighted average around a given finite element e is calculated from the values associated with a list of finite elements v surrounding e. This list of finite elements surrounding e is based on a sphere, with a radius noted r_{minc} in the case of filtering $\frac{\partial \tilde{C}}{\partial \rho_e}$ and noted r_{mind} in the case of filtering ρ_e. These radii can be changed independently to locally enlarge or shrink the associated filter. It is important to underline that these filters are applied on design elements only and that non-design elements located inside a sphere and are not taken into account in weighted average.

Thus, if N_e elements are surrounding element e (including element e itself), the filtered value of $\frac{\partial \tilde{C}}{\partial \rho_e}$, noted $\overline{\frac{\partial \tilde{C}}{\partial \rho_e}}$ is calculated as $\overline{\frac{\partial \tilde{C}}{\partial \rho_e}} = \frac{1}{\frac{\rho_e}{V_e}} . \frac{\sum_{v=1}^{N_e} H_v . \frac{\rho_v}{V_v} . \frac{\partial \tilde{C}}{\partial \rho_v}}{\sum_{v=1}^{N_e} H_v}$

Where the weight H_v is given by the linearly decaying function: $H_v = (r_{minc} - r_v)^k$
$r_v = dist(e, v)$ *is the distance between the centers of elements e and v.*
k is a empiric coefficient used to intensify the effect of r_v. ($k = 1$ *has been used for all results presented in this paper*).
V_e *is the actual volume of element e.*
Filtering of ρ_e, designed as $\bar{\rho_e}$ is performed using $\bar{\rho_e} = \frac{\sum_{v=1}^{N_e} \omega_v . \rho_v}{\sum_{v=1}^{N_e} \omega_v}$

Where the weight ω_v is Gaussian and given by $\omega_v = V_v . \frac{exp\left(-\frac{r_v^2}{2.\left(\frac{r_{mind}}{3}\right)^2}\right)}{2.\pi.\left(\frac{r_{mind}}{3}\right)}$

V_v *is the actual volume of element v.*

If compared with the equations used in the context of structured meshes, the main difference relies on the fact that, due to significantly varying element sizes, we had to introduce the element volumes V_v in these two filters. Fig. 8 shows 8 stages in the evolution of $\rho(x, y, z)$ for the same example as in Fig. 6, with filtering applied on $\frac{\partial \tilde{C}}{\partial \rho_e}$ (with $r_{minc} = 1.25\,\delta$ where δ is the local value of the tetrahedron size, which is nearly constant across the mesh in this case).

Then, Fig. 9 also shows 8 stages in the evolution of $\rho(x, y, z)$ for the same example, with filtering applied on ρ_e (with $r_{mind} = 1.25\,\delta$).

A comparison between these results (Fig. 6, Fig. 8, Fig. 9 and Table 1) leads to the following general conclusions in the context of 3D unstructured meshes:

- The relative density distribution $\rho(x, y, z)$ and by the way the optimized shape and topology is significantly influenced by filtering
- Results obtained using one or the other type of filter can be quite different
- When a filter on ρ_e is applied, the final distribution of $\rho(x, y, z)$ becomes more diffuse or less "binary" but as well it becomes smoother.
- Both types of filters, if applied with correct parameters, tend to eliminate checkerboard effects but they also seem to weaken the results obtained as the final compliance increases. These filters a priori seem to move the solution away from the theoretical optimum (with the lowest compliance) which involves checkerboard effects, but this is not true. This type of optimum is indeed not physical (in addition to not being practical). As very well explained by Bensoe [2], checkerboard solutions feature artificially high stiffness because, in

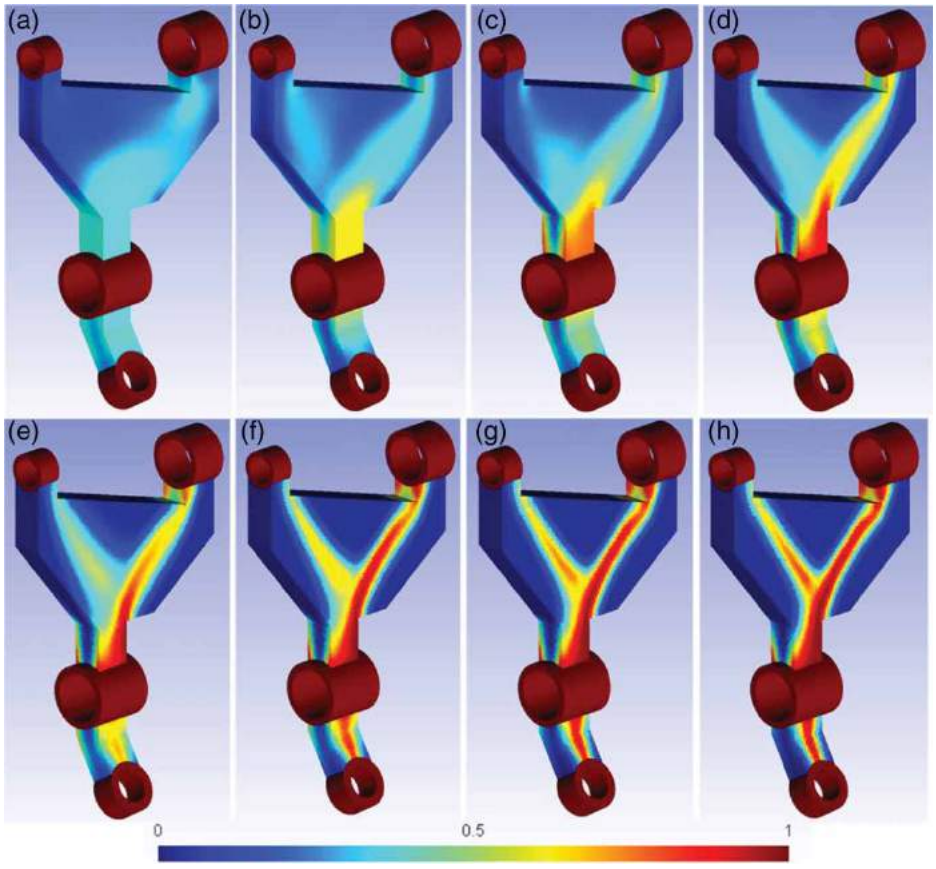

Fig. 9: Evolution of $\rho(x, y, z)$ for the example in Fig. 5, after (a) 1 iteration (b) 2 iterations (c) 3 iterations (d) 5 iterations (e) 7 iterations (f) 11 iterations (g) 15 iterations (h) 21 iterations (with a filter on ρ_e applied).

the SIMP process, they are analyzed using FEA discrete formulations for which the Babuska-Brezzi numerical stability condition is not satisfied.

3.5. Generation of an Optimized 3D Geometry

As mentioned in the previous section, the raw result of the SIMP method is a relative density distribution across the initial mesh. This distribution has, in itself, only little significance for design purposes and it requires further processing. Two main approaches can be identified when trying to generate an optimized 3D geometry from raw SIMP results:

- Considering a threshold ρ_{min} on the distribution of $\rho(x, y, z)$ and keeping all finite elements (tetrahedrons here) for which $1 \geq \rho(x, y, z) > \rho_{min}$. In this case, as illustrated just below, the exterior boundary of the optimized design is composed with a very irregular triangulation, which requires the removal of non-manifold patterns along with a significant smoothing (not detailed in this paper). At this point of our work, this smoothing is based on the algorithm presented in [5]. When applied on distributions of $\rho(x, y, z)$ featuring checkerboard effects (without smoothing), this alternative leads to very fascinating images (see Fig. 10) that illustrate the final impact of the checkerboard effect on 3D unstructured meshes and by the way, why they have to be avoided. Fig. 11 shows, for 2 values of ρ_{min} on the result illustrated in Fig. 8h (with filtering applied on $\frac{\partial \tilde{C}}{\partial \rho_e}$), 3D optimized shapes obtained using this alternative, before and after removing non-manifold patterns and smoothing. For comparison, Fig. 12 shows the optimized shapes obtained on the result illustrated in Fig. 9h (with filtering applied on ρ_e).
- Computing iso-density (iso-ρ) surfaces from a continuous approximation of $\rho(x, y, z)$. This alternative first require transforming the original distribution $\rho(x, y, z)$ into a continuous distribution $\rho^*(x, y, z)$. Indeed, due to Young's Modulus penalization, $\rho(x, y, z)$ is classically constant across each finite element. A continuous field $\rho^*(x, y, z)$ can be easily computed using linear piecewise interpolation inside each finite element from nodal values of $\rho(x, y, z)$ calculated with a weighted average of surrounding elements' relative density. Once $\rho^*(x, y, z)$ obtained,

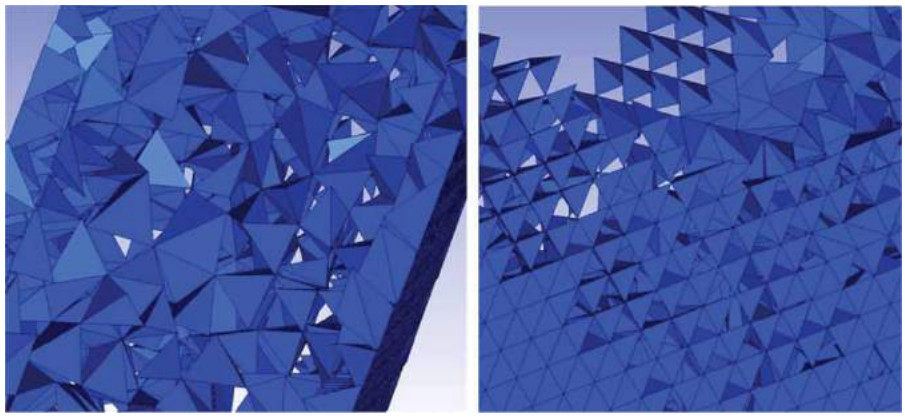

Fig. 10: Two examples of the final impact of checkerboard effects on 3D unstructured meshes.

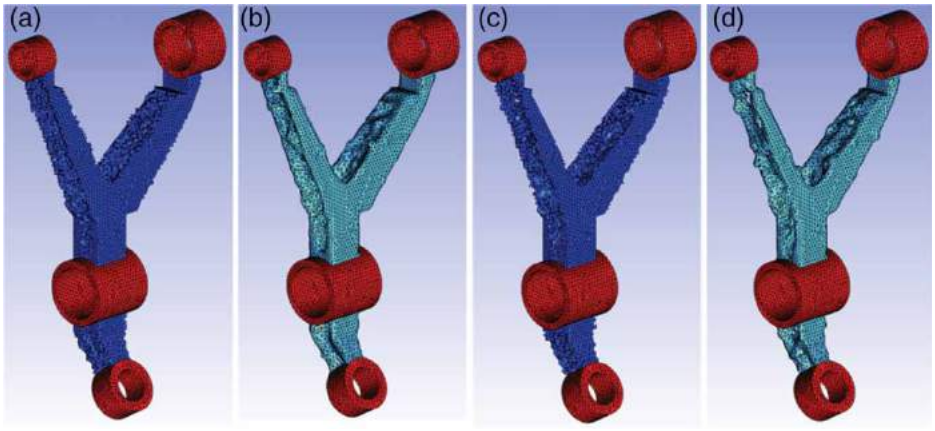

Fig. 11: First alternative: final shapes derived from $\rho(x, y, z)$ in Fig. 8h before and after smoothing (a) and (b) $\rho_{min} = 0.2$ (c) and (d) $\rho_{min} = 0.4$.

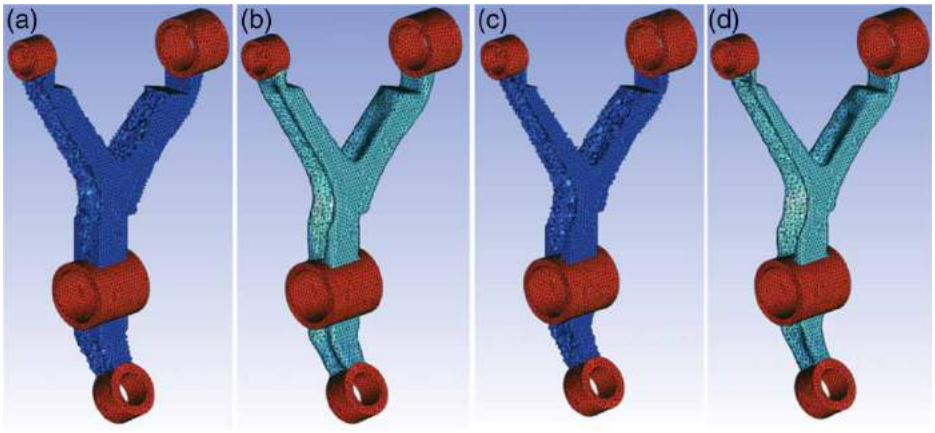

Fig. 12: First alternative: final shapes derived from $\rho(x, y, z)$ in Fig. 9h before and after smoothing (a) and (b) $\rho_{min} = 0.2$ (c) and (d) $\rho_{min} = 0.4$.

iso-density surfaces defined by $\rho^*(x, y, z) = \rho_{min}$ can be computed as a triangulation. Even if boundary triangulations derived this way are a lot smoother than those derived with the first alternative, they are also smoothed using the algorithm presented in [5]. Obviously, as this second alternative is based on computing a continuous distribution of $\rho(x, y, z)$, it leads to much better results when a filter on ρ_e is applied. Fig. 13 shows the optimized shapes obtained using this second alternative for the same 2 values of ρ_{min} on the example shown in Fig. 9h.

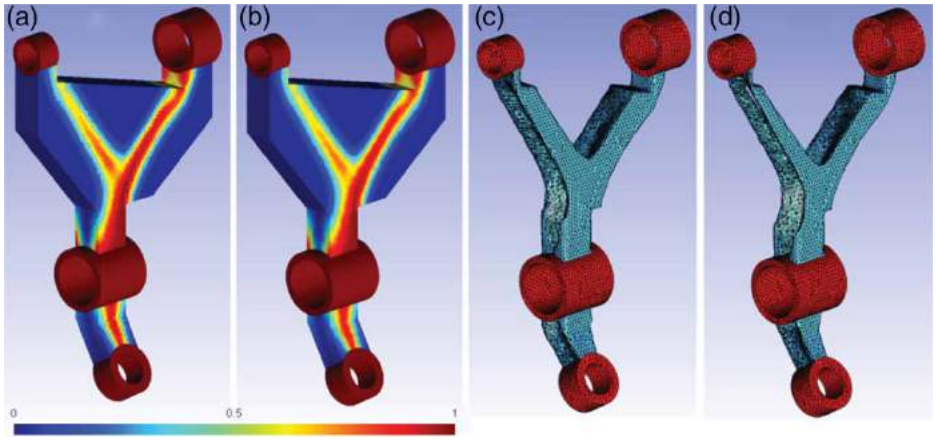

Fig. 13: Second alternative: from $\rho(x,y,z)$ in Fig. 9h (a) The distribution of $\rho(x,y,z)$ (b) The distribution of $\rho^*(x,y,z)$ and final shapes derived (c) with $\rho_{min} = 0.2$ (d) with $\rho_{min} = 0.4$.

The comparison between shapes introduced in Fig. 11 and Fig. 12 shows that filtering ρ_e leads to smoother and in general more compact optimized shapes. Practically, the major drawback of filtering ρ_e instead of $\frac{\partial \tilde{C}}{\partial \rho_e}$ is that setting up ρ_{min} is a little more delicate because, as mentioned earlier, the distribution of $\rho(x,y,z)$ is more diffuse. Indeed, the final objective remains fulfilling the condition $\tilde{V}(\rho) = f.V_d$ and consequently, the value of ρ_{min} should be adjusted so that the actual optimized design volume equals $f.V_d$. In most cases the adjusted value of ρ_{min} is close to $\rho_{min} = 0.4$. When no filtering is applied along the SIMP process, the final distribution of $\rho(x,y,z)$ is close to binary. Consequently, the effect of ρ_{min} on the optimized design volume is negligible in this case but we have seen that it leads to unpractical results due to checkerboard effects. An interesting study of the effect of ρ_{min} on optimization results for 2D shapes can be found in [11]. Then, the comparison between Fig. 12 and Fig. 13 illustrates that, when applied to SIMP results where ρ_e has been filtered, the two alternatives (applying a threshold on $\rho(x,y,z)$ or computing iso-ρ surfaces) lead to very similar results.

4. PRACTICAL EXAMPLES AND CHALLENGES

The framework described along this paper has been successfully implemented through the design of a TO platform based on C++ code and on the use of Code_Aster™ as a FEA solver. We used Gmsh™ [10] for visualizing meshes and SIMP results. The process is fully automated, starting from the input of the two B-Rep models mentioned previously along with loads, BC, and SIMP parameters, and ending with an optimized 3D geometry (as a triangulated B-Rep or STL file). In the following paragraphs, in order to illustrate challenges inherent to the practical integration of TO with CAD, we present an application of our method to a set of optimization problems.

4.1. First Example: a "Sitting Device"

The first model is illustrated in Fig. 14. A vertical load (resultant force F_v) and an horizontal load (resultant force F_h) are applied while the model is anchored to the ground on 4 locations. Filtering on ρ_e is applied, the first alternative is used for computing the optimized 3D shape and ρ_{min} is adjusted to fulfil the target on f. Fig. 15a shows the optimized shape obtained with $F_h = 2.F_v$ and $f = 0.03$, Fig. 15b with $F_h = 2.F_v$ and a mesh with smaller elements and Fig. 15c with $F_h = 10.F_v$ and $f = 0.03$. This example illustrates well the potential of the integration of TO with CAD towards the automatic generation of new designs but also some of the practical problems that can be faced. Indeed, the optimized shape obtained in Fig. 15a is not symmetric despite the fact that the optimization problem is symmetric and that the design intent is obviously generating a symmetric shape. The only potential source of asymmetry in the problem is the unstructured mesh itself. Fig. 16 illustrates the evolution of $\rho(x,y,z)$ through SIMP iterations on both sides of the domain and the occurrence of asymmetry in the solution. Thus, a very tiny difference in the mesh between the right and left sides of the domain is likely to result in a significant difference in the final solution and by the way in the final design.

This example illustrates how sensitive the optimization process can be with respect to the mesh used, specifically to the element size and quality distribution. This type of problems can usually be avoided using a mesh with smaller elements. Indeed, Fig. 15a shows the asymmetric solution obtained with a constant mesh size equal to 0.5 while Fig. 15c shows a symmetric solution obtained with a constant mesh size equal to 0.35. Moreover, like in FEA in general, overcoming asymmetry problems can be easily done by modeling one half of the domain. This approach is used by commercial optimization software (Inspire by for example) for the implementation of *manufacturing constraints* such as *symmetry*,

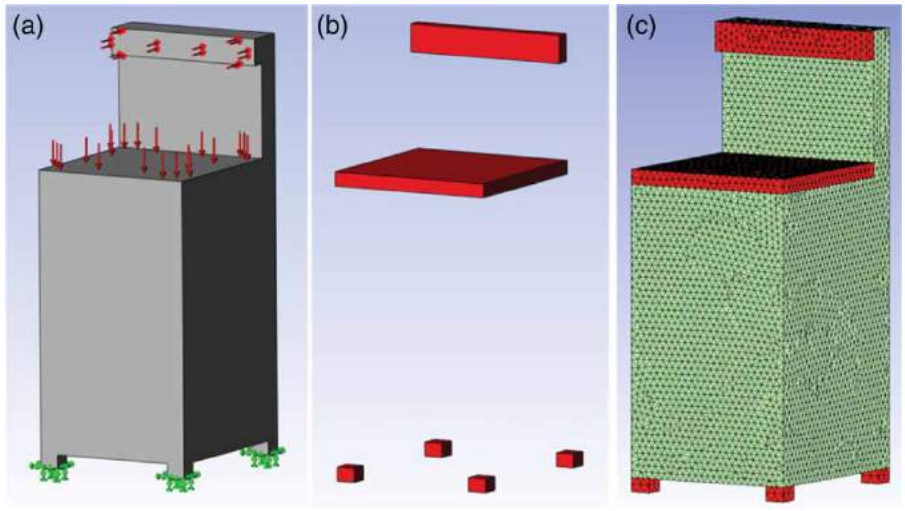

Fig. 14: First example (sitting device): (a) the entire domain with loads and BC, (b) the non-design sub-domain, (c) the resulting heterogeneous mesh.

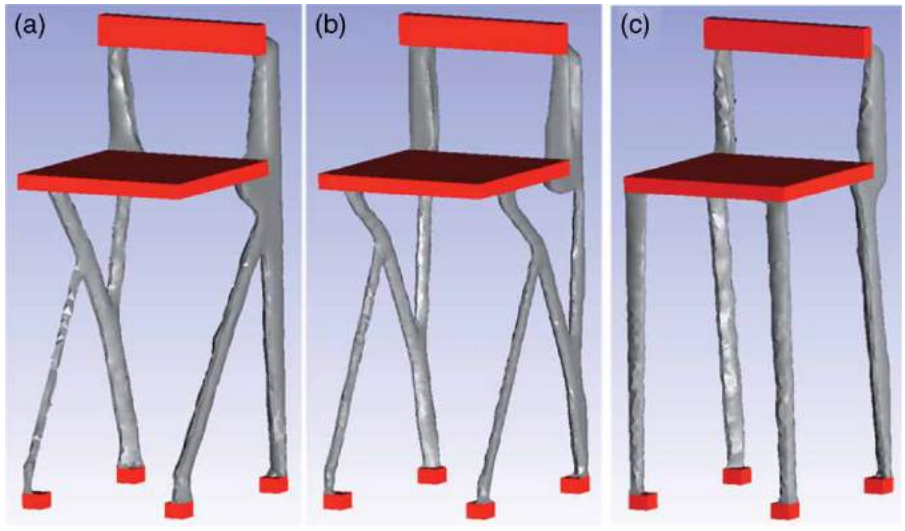

Fig. 15: First example (a) The optimized shape with $F_h = 2.F_v$ and $f = 0.03$ (b) The optimized shape with $F_h = 2.F_v$, $f = 0.03$ and smaller elements (c) The optimized shape with $F_h = 10.F_v$ and $f = 0.03$.

pattern repetition and *cyclic repetition* (as referred to in Inspire). This example also shows (when comparing Fig. 15a with Fig. 15b) that, as it could be anticipated, the optimized shape is strongly influenced by the balance of loads applied.

4.2. Second example: a "supporting device"

The second model (Fig. 17) is anchored to the ground on 4 locations and a vertical load is applied on 4 locations. Filtering on ρ_e is applied, the first alternative is used for computing the optimized 3D shape and ρ_{min} is adjusted to fulfill the target on f. The results (Fig. 18) illustrate well how powerful the integration of TO can be towards the automatic creation of new designs. However, the results obtained cannot be used practically as the optimized designs, if used as is, are likely to fail by buckling. Potentially irrelevant results like these derive from the fact that standard FEA, on which SIMP iterations are based, does not a priori take buckling (or other phenomenon) into account. In this type of situations, further investigations should be made, which represents challenges towards the full automation of design creation through the integration of TO with CAD.

4.3. Third Example: a "Mounting Device"

For the third example (Fig. 19) the central hole is loaded and the four mounting holes attached. Filtering on ρ_e is applied, the first alternative is used for computing the optimized 3D shape and ρ_{min} is

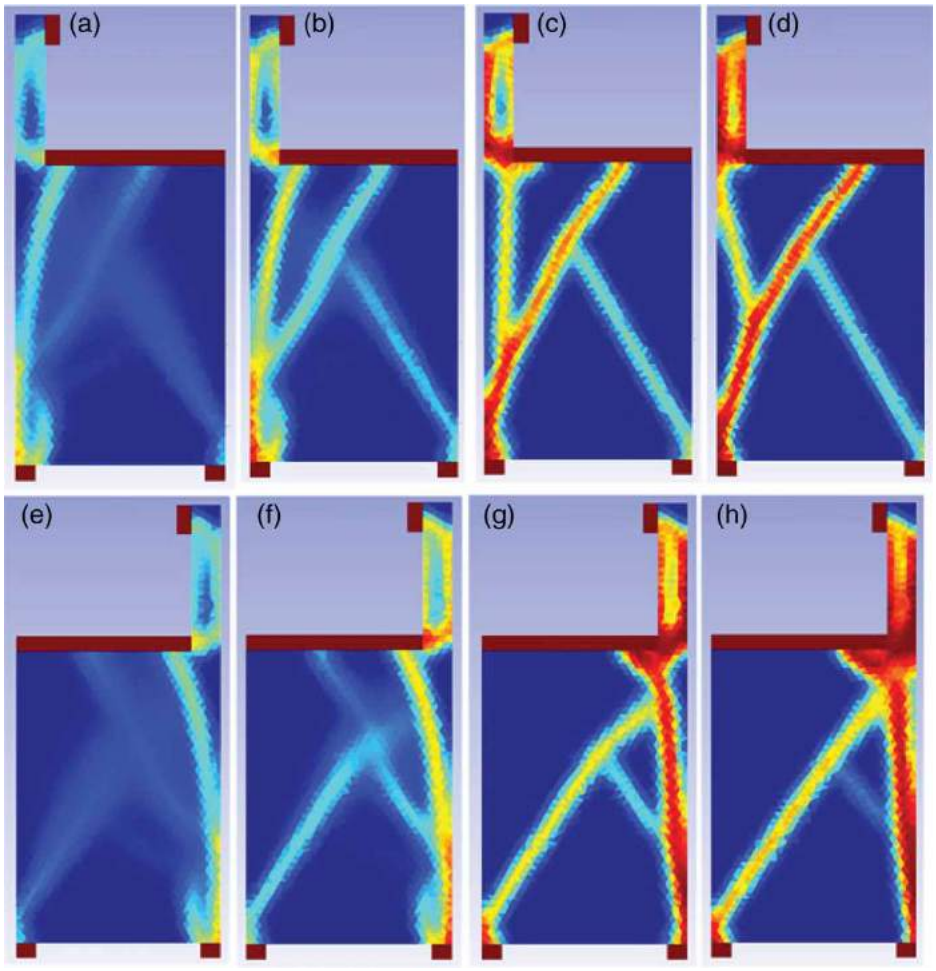

Fig. 16: $\rho(x, y, z)$ at iterations 8,9,10 for the first example (a) (b) (c) (d) On the right side of the domain (e) (f) (g) (h) On the left side of the domain.

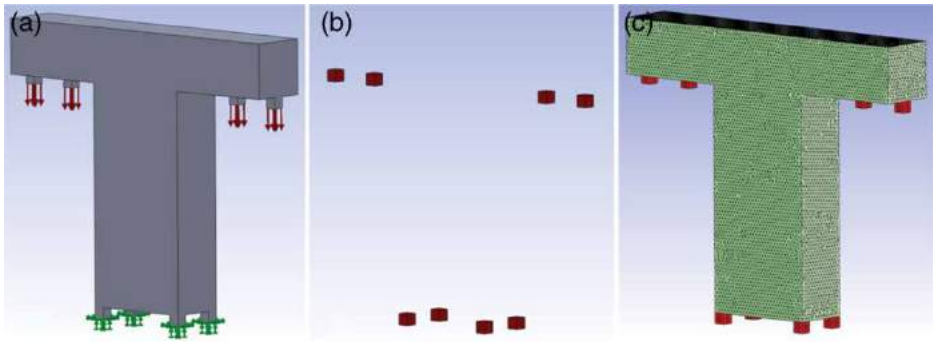

Fig. 17: Second example (supporting device): (a) the entire domain with loads and BC, (b) the non-design sub-domain, (c) the resulting heterogeneous mesh.

adjusted to fulfill the target on f. The final result obtained with $f = 0.1$ and a constant mesh size equal to 0.15 is shown in Fig. 20a. This figure illustrates another problem when using TO since two mounting holes are not linked to the central bore. This optimized shape is theoretically viable but not practically acceptable. This type of situations is related to similar issues as mentioned in the first example. Indeed, the unstructured mesh is not perfectly symmetric, which is likely to bring about uncertainty with respect to the optimized shape obtained at the end. In fact, at some point along SIMP iterations, the solution can

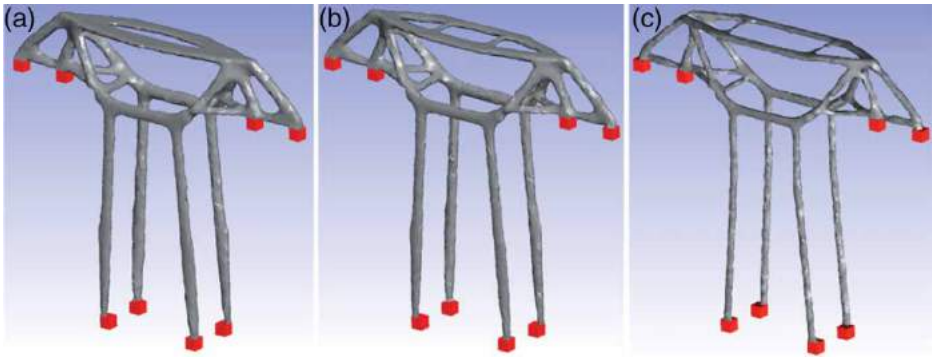

Fig. 18: Second example (supporting device) optimized shapes (a) $f = 0.07$ (b) $f = 0.06$ (c) $f = 0.04$.

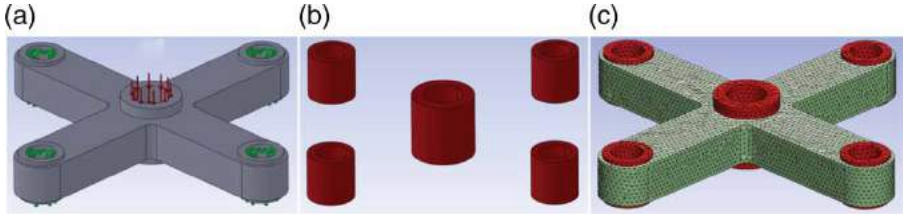

Fig. 19: Third example (mounting device) (a) The entire domain with loads and BC (b) The non-design sub-domain (c) The resulting heterogeneous mesh.

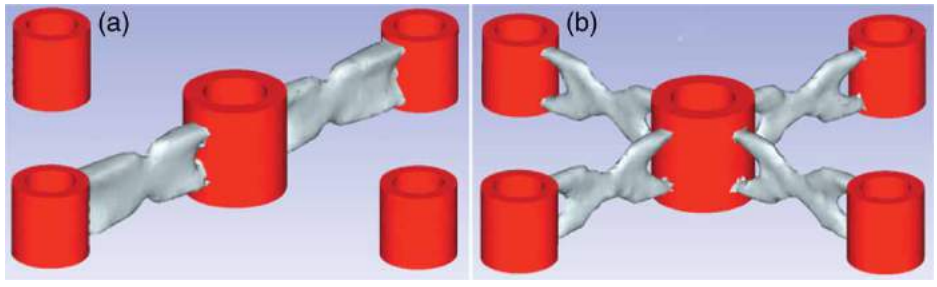

Fig. 20: Third example (mounting device), optimized shape (a) f = 0.1 and mesh size = 0.15 (b) f = 0.1 and mesh size = 0.125.

take one direction or another which may induce a loss in material continuity. Decreasing element size can solve the problem as illustrated in Fig. 20b. However, it is difficult to "a priori" set up mesh size in order to guarantee avoiding this type of problems. The fact that, at some point along SIMP iterations, there is a change in the way the design material is connected can be detected by looking at the evolution of $\Delta_i = \frac{\tilde{C}_i - \tilde{C}_{i-1}}{\tilde{C}_{i-1}}$.

Fig. 21 illustrates, for the example in Fig. 20a, the evolution of Δ_i along SIMP iterations, while Fig. 22 illustrates this evolution for the example in Fig. 20b. As shown in these two figures, each change in the design material's structure is reflected by a significant increase of Δ_i for a few iterations. Thus, the appearance of a loss in material continuity in Fig. 20a is clearly reflected in the evolution of Δ_i in Fig. 25 (iteration 19). Losses in material continuity lead to irrelevant optimized shapes. With the objective of automating the whole process, a potential solution consists of automatically detecting losses of material continuity and decreasing the element size. Another solution is introducing a material continuity constraint into the TO process itself. This can be done quite easily when using ESO and BESO topology optimization methods but it is much more delicate with the SIMP method.

4.4. Fourth Example: a "Bearing Bracket"

The fourth and last model considered is a bearing bracket, which is illustrated with loads applied (a combination of vertical and horizontal forces) in Fig. 23. With this example, our intent is showing that the choice of BC, along with associated non-design geometry, has a very significant impact on optimized shapes created. For this, we consider three cases (referred to as cases 1,2 and 3) depending on the way displacements are imposed on the model to represent the flat contact under the bracket's bottom flange. For

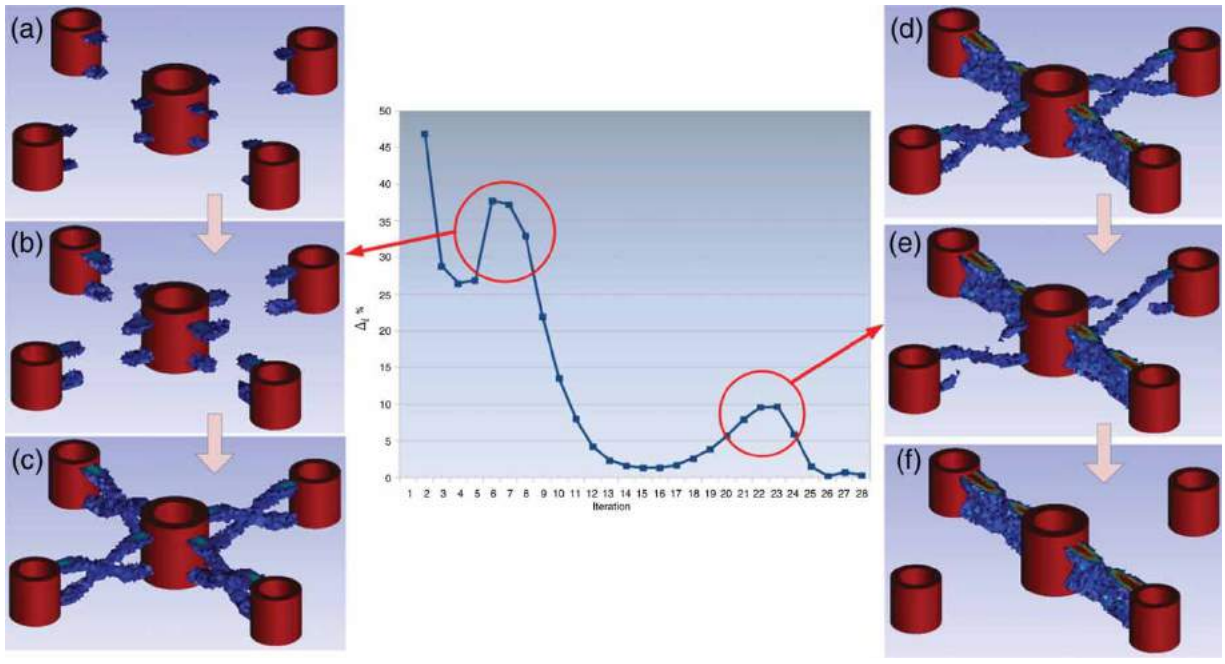

Fig. 21: The evolution of Δ_i and the optimized shape for the example in Fig. 20a after (a) 3 iterations (b) 5 iterations (c) 6 iterations (d) 18 iterations (e) 19 iterations (f) 21 iterations.

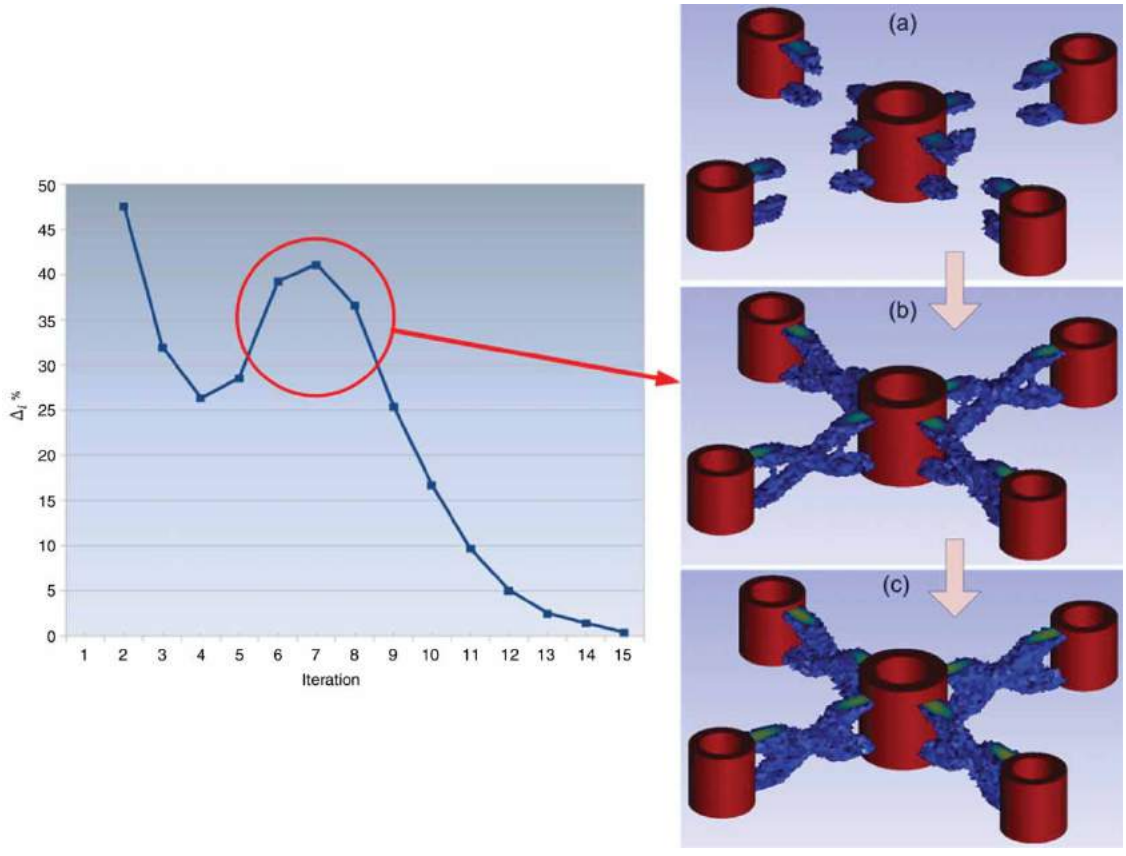

Fig. 22: The evolution of Δ_i and the optimized shape for the example in Fig. 20b after (a) 5 iterations (b) 6 iterations (c) 7 iterations.

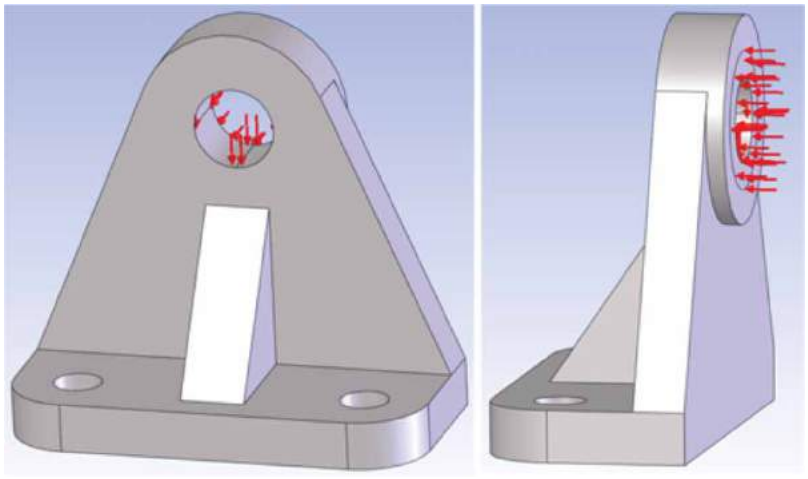

Fig. 23: Fourth example (bearing bracket) and loads applied.

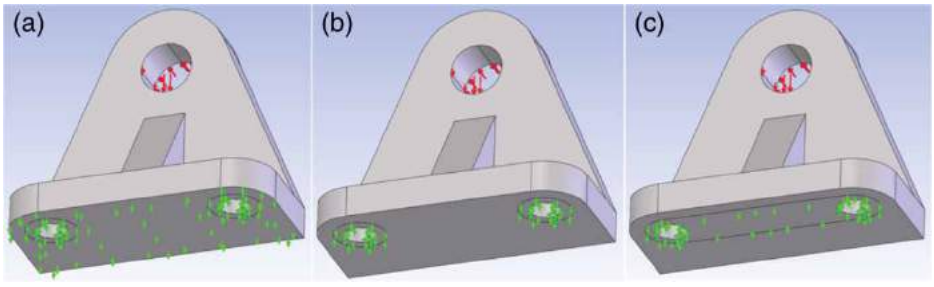

Fig. 24: Displacements imposed to the bearing bracket: (a) first case, (b) second case, (c) third case.

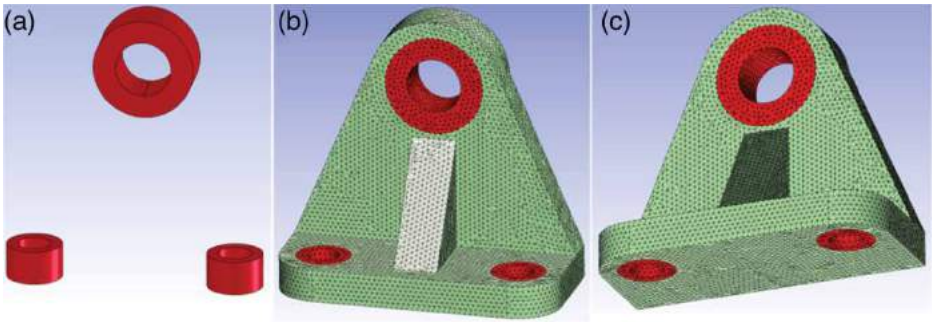

Fig. 25: Bearing bracket, first and second cases: (a) the non-design sub domain, (b) (c) the resulting heterogeneous mesh.

the three cases, bolting is represented by blocking the two mounting holes. Considering the flat contact, for the first case, a null displacement is applied on the whole inferior face (Fig. 24a) whereas for the second case, it is only applied on two annular faces around holes (Fig. 24b). For the third case, the null displacement condition is applied on a sub-face surrounding the two holes as shown in Fig. 24c.

Fig. 25 and Fig. 26 introduce non-design subdomains used for these three cases along with resulting meshes. Thus, the flat contact surface under the bracket's bottom flange is likely to evolve for the first case only. It is worth underlining that the second case is the most conservative because the contact surface considered is smaller than the optimized part's actual contact surface. Fig. 27 and Fig. 28 summarize optimization results obtained for the first two cases using three values for the target volume fraction f. For the third case (Fig. 29), due to the non-design volume increase, the target volume fractions f have been decreased so that the optimized volumes are the same as for the first two cases.

Results obtained for the three cases considered are obviously quite different, which underlines the impact

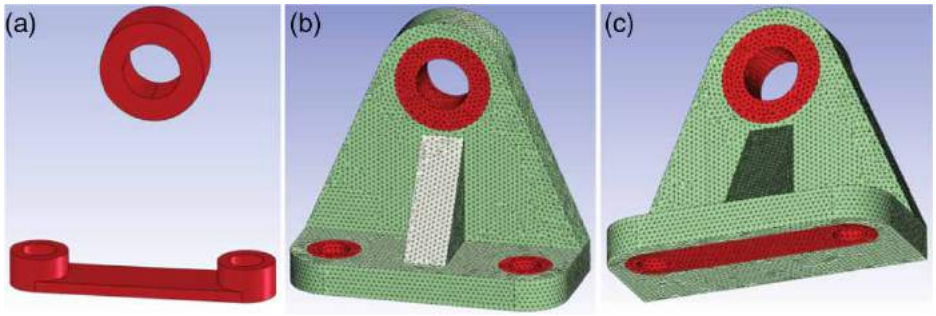

Fig. 26: Bearing bracket, third case: (a) the non-design sub domain, (b) (c) the resulting heterogeneous mesh.

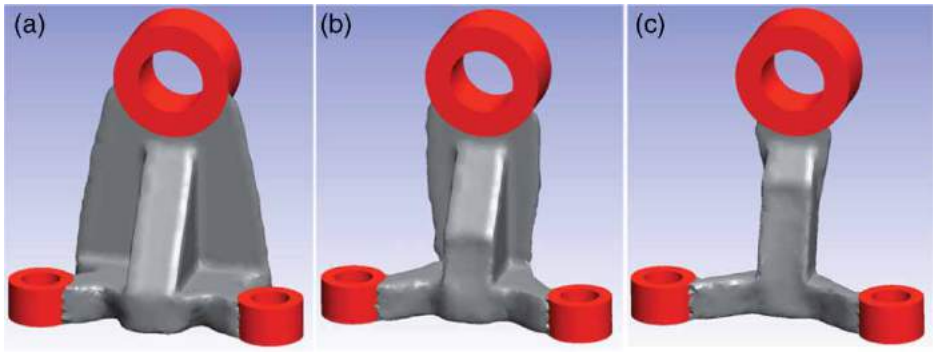

Fig. 27: Optimized shapes (bearing bracket) for the first case: (a) f = 0.3, (b) f = 0.2, (c) f = 0.1.

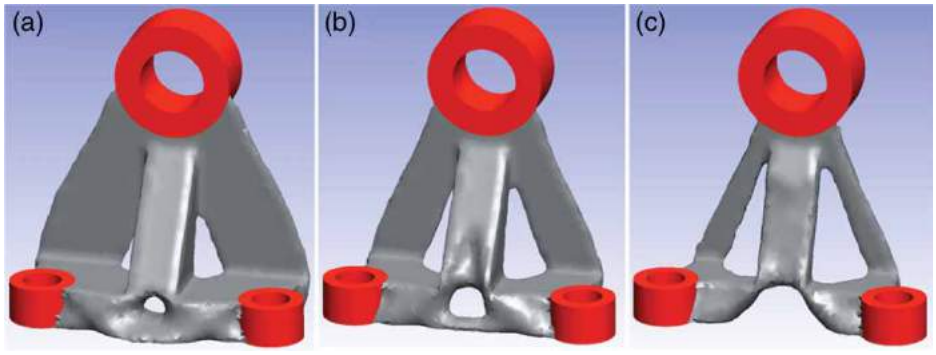

Fig. 28: Optimized shapes (bearing bracket) for the second case: (a) f = 0.3, (b) f = 0.2, (c) f = 0.1.

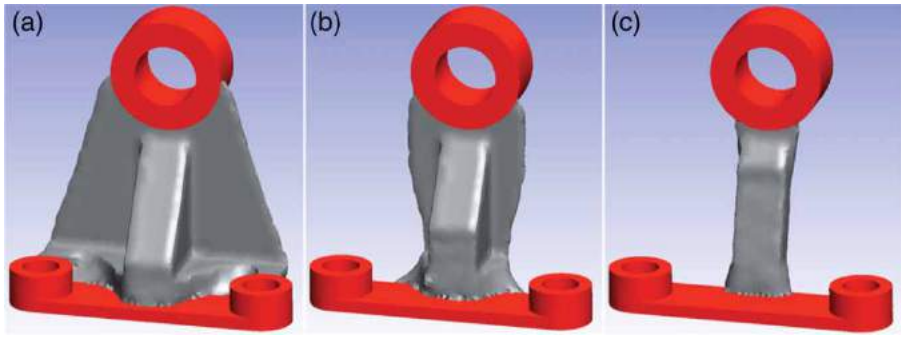

Fig. 29: Optimized shapes (bearing bracket) for the third case: (a) f = 0.272, (b) f = 0.168, (c) f = 0.064.

of BC on optimized shapes. The choice of BC may be sensitive for any FEA but St-Venant's principle makes that a priori quite different sets of BC may, at the end, lead to the same FEA conclusions in locations of interest. When using FEA for TO, this is not true anymore and a priori quite different combinations of BC and

non-design sub-domains usually lead to quite different optimization results. Moreover, as it is the case for this example, introducing contact conditions along with specific connectors can be the most appropriate way to impose BC, which increases analysis complexity by introducing nonlinearity. In general, modeling loads, BC and non-design geometry mixed with an evolving shape is part of the most sensitive problems faced in the practical use of TO.

5. CONCLUSION AND PERSPECTIVES

The integration between geometric modeling, automatic unstructured mesh generation and TO represents a promising step forward and the examples presented show its huge potential in the context of product development. Nevertheless, these examples also underline that a lot of research work remains to be done to make this integration actually efficient with a practical perspective. The practical specification of *non-design sub-domains* can be improved but this is not a major issue if compared to the problems pointed out in section 4. Using meshes with varying element sizes and integrating other TOM could represent promising ideas towards further developments and enhancements. Indeed, one of the most important drawbacks of the SIMP method is that is does not explicitly involve the optimization of stress distribution, which is usually the most sensitive issue when trying to optimize a mechanical design. The fact that the framework presented in this paper has been built with the objective of being able to easily integrate and mix any shape and TOM, brings about very interesting perspectives. The automatic (or at least assisted) creation of a CAD model of the final optimized shape from the results provided by the SIMP method is also a natural perspective for further research work on the subject. Many approaches can be foreseen in this objective but automating the construction of CAD models from TO result is, at this point, still extremely ambitious and it is clearly a long term perspective. One of the major challenges in this latter direction is introducing a manufacturing perspective into the process. Indeed, building a consistent optimized shape is not only a matter of compliance and stress distribution but also a matter of manufacturability.

ACKNOWLEDGEMENTS

This study was carried out as part of a project supported by research funding from the Québec Nature and Technology Research Fund and by the Natural Sciences and Engineering Research Council of Canada (NSERC).

REFERENCES

[1] Bendsøe, M.P.; Kikuchi, N.: Generating optimal topologies in structural design using a homogenization method. Computer Methods in Applied Mechanics and Engineering, 71(2), 1988, 197–224. http://dx.doi.org/10.1016/0045-7825(88)90086-2

[2] Bendsoe, M.P.; Sigmund, O.: Topology optimization - Theory,Methods and Applications, 2nd ed. 2003, Berlin: Springer. 370.

[3] Bourdin, B.: Filters in topology optimization, International Journal for Numerical Methods in Engineering, 50(9), 2001, 2143–2158.

[4] Bruns, T.E.: A reevaluation of the SIMP method with filtering and an alternative formulation for solid-void topology optimization, Struct. Multidisc. Optim., 30, 2005, 428–436. http://dx.doi.org/10.1007/s00158-005-0537-x

[5] Chen, C.-Y.; Cheng, K.-Y.: A direction-oriented sharpness dependent filter for 3D polygon meshes, Computers & Graphics, 32(2), 2008, 129–140. http://dx.doi.org/10.1016/j.cag.2008.02.002

[6] Chen, J., et al.: Shape optimization with topological changes and parametric control, International Journal for Numerical Methods in Engineering, 71(3), 2007, 313–346. http://dx.doi.org/10.1002/nme.1943

[7] Cugini, U., et al.: Integrated Computer-Aided Innovation: The PROSIT approach, Computers in Industry, 60, 2009, 629–641. http://dx.doi.org/10.1016/j.compind.2009.05.014

[8] Cuillière, J.-C.; François, V.; Drouet, J.-M.: Automatic mesh generation and transformation for topology optimization methods, Computer-Aided Design, 45(12), 2013, 1489–1506. http://dx.doi.org/10.1016/j.cad.2013.07.004

[9] Frey, P.J.; George, P.-L.: Mesh generation: Application to finite elements, ed. Wiley. 2008.

[10] Geuzaine, C.; Remacle, J.-F.: Gmsh: a three-dimensional finite element mesh generator with built-in pre- and post-processing facilities, International Journal for Numerical Methods in Engineering, 79(11), 2009, 1309–1331. http://dx.doi.org/10.1002/nme.2579

[11] Hsu, M.-H.; Hsu, Y.-L.: Interpreting three-dimensional structural topology optimization results, Computers & Structures, 83(4-5), 2005, 327–337.

[12] Huang, X.; Xie, Y. M.; Burry, M. C.: Advantages of bi-directional evolutionary structural optimization (BESO) over evolutionary structural optimization (ESO), Advances in Structural Engineering, 10(6), 2007, 727–737. http://dx.doi.org/10.1260/136943307783571436

[13] Juretic, F.: Conformal Meshing of Multiple Domains in Contact, in International Meshing Roundtable, 2008: Pittsburgh.

[14] Mantyla, M.: An introduction to solid modeling, ed. C.S. Press. 1988.

[15] Norato, J., et al.: A geometry projection method for shape optimization, Int. J. for

Numerical Methods in Engineering, 60(14), 2004, 2289–2312. http://dx.doi.org/10.1002/nme.1044

[16] Sigmund, O.: On the design of compliant mechanisms using topology optimization, Mechanics of Structures and Machines, 25(4), 1997, 493–524. http://dx.doi.org/10.1080/08905459708945415

[17] Sigmund, O.: Morphology-based black and white filters for topology optimization, Structural and Multidisciplinary Optimization, 33(4-5), 2007, 401–424. http://dx.doi.org/10.1007/s00158-006-0087-x

[18] Sigmund, O.; Petersson, J.: Numerical instabilities in topology optimization: A survey on procedures dealing with checkerboards, mesh-dependencies and local minima, Structural Optimization, 16, 1998, 68–75. http://dx.doi.org/10.1007/BF01214002

[19] Victoria, M.; Querin, O. M.; Martí, P.: Topology design for multiple loading conditions of continuum structures using isolines and isosurfaces, Finite Elements in Analysis and Design, 46(3), 2010, 229–237. http://dx.doi.org/10.1016/j.finel.2009.09.003

[20] Zhang, Y.; Hughes, T. J. T.; Bajaj, C. L.: An automatic 3D mesh generation method for domains with multiple materials, Computer Methods in Applied Mechanics and Engineering, 199(5-8), 2010, 405–415. http://dx.doi.org/10.1016/j.cma.2009.06.007PMid:20161555PMCid:2805160